BMC Gastroenterology

RESEARCH

Open Access

Sodium butyrate entrapped chitosan-PAMAM for suppression of colorectal cancer cells

Ruaa Mahdi Mayih Al-Zihaymee[1], Javad Mohammadnejad[2*], Asghar Narmani[3], Hanieh Jafar[1], Gülüzar Özbolat[4], Amin Daemi[5*], Yusuf Döğüş[5] and Seyyedeh Touran Hosseini[6]

Abstract

Objective Cancer treatment is a major concern of health worldwide. Nowadays, colorectal cancer is one of the most prevalent diseases throughout the globe. Therefore, novel cancer treatment modalities are required to stop cancer. Thus, this paper aims to develop a novel drug delivery system (DDS) based on Chitosan (CS), polyamidoamine (PAMAM G4), and Nanoparticles (NP) for efficient delivery of sodium butyrate (NB) and Fe_2O_3 to SW480 colorectal cancer cells.

Methods To do so, after characterizing the nanocarrier with FT-IR, DLS, TEM, and TGA, nanometric size (40-65 nm), high drug content (23% Fe_2O_3 and 3% NB), controlled NB release (4% within 2 h), and pH-sensitive NB release (35% within 2 h) were measured for CS-PAMAM-Fe_2O_3-NB.

Result In biomedical tests, MTT assay indicated 10% (after 24 h), 8% (after 48 h), and 7% (after 72 h) cell viabilities for 200 nM concentration of CS-PAMAM-Fe_2O_3-NB nanocarrier on SW480 cells while pure NB did not have potential toxicity on cancer cells. IC_{50} determined for 25 nM after 24 h. qRT-PCR test indicated a 7-fold and 10-fold increase for Caspase9 and Bax apoptotic genes whereas 0.3-fold expression quantified for Bcl2 anti-apoptotic gene.

Conclusion According to the obtained results, it can be concluded that the fabricated nanocarrier would be a potential DDS against colorectal cancer cells. The results of these biomedical tests have approved potential the ability of the synthesized DDS in the inhibition of colorectal cancer cells. High biocompatibility was shown in MSC normal cells which further verified the efficiency of CS-PAMAM-Fe_2O_3-NB.

Keywords PAMAM-Chitosan nanoparticles, Fe_2O_3 nanoparticles, Sodium butyrate, Controlled drug release, Colorectal cancer inhibition

*Correspondence:
Javad Mohammadnejad
mohamadnejad@ut.ac.ir
Amin Daemi
phd_bio@ahoo.com
[1]Department of Biology, SR.C., Islamic Azad University, Tehran, Iran
[2]Department of Nanobiotechnology and Biomimetic, School of Life Science Engineering, College of Interdisciplinary Science and Technology, University of Tehran, Tehran, Iran
[3]Department of Medical Nanotechnology, School of Advanced Technologies in Medicine, Tehran University of Medical Sciences, Tehran 14177-55469, Iran
[4]Faculty of Health Science, Sinop University, Sinop, Turkey
[5]Department of Medical Biochemistry, Faculty of Medicine, Cukurova University, Adana, Turkey
[6]Department of Biotechnology, Institute of Natural and Applied Sciences, Cukurova University, Adana, Turkey

Introduction

Colorectal cancer, the third leading cause of cancer death throughout the globe, has a high rate of incidence. The ever-increasing rate of this cancer is going to make a big health-related problem for human beings [1, 2]. This adenocarcinoma originates from the epithelial cells of the large intestine when genetic or epigenetic mutations take place in certain epithelium cells. The high proliferation rate of cells can result in the generation of benign adenoma that subsequently, may progress and form carcinoma and cause metastasis [3]. According to statistics, colorectal cancer accounts for about 10% of cancer incidence and 9.4% of deaths in 2020 all around the world. It has been predicted that approximately 3.2 million deaths will be occurring as a result of colorectal cancer in 2040 [4]. Lifestyle and diet toward westernization are the main environmental risk factors correlated with this cancer incidence and death. There are sort of modalities called conventional or traditional approaches in cancer therapy, including surgery, hormone therapy, hormone therapy, immunotherapy, chemotherapy, and radiotherapy, which applied for the suppression of cancer incidence during the last decades; however, several deficiencies associated with these modalities, such as long-term treatment, poor repeatability, low specificity, weak stability, high side effects, inefficient recovery of patients after treatment, less cost-effectiveness, immunogenicity, etc., have mentioned as limitations of these approaches in diagnosis and treatment of colon cancer [5–10].

As a result, new breakthrough technologies must be applied to introduce novel treatment approaches for the suppression and efficient treatment of cancer and ignore the drawbacks of conventional approaches. One of the most practical and efficient approaches is using nanoparticle (NP)-based drug delivery systems (DDSs) in which nanotechnology concepts and properties apply for gaining excellent output in cancer treatment [11, 12]. Physicochemical aspects of NPs, like high surface-to-volume ratio, good stability, high solubility, thermal features, ease of manipulation, and so forth are the major advantages of NPs in DDS. In this way, Ren et al. [13] developed an emodin-conjugated pegylation of FE3O4 nanoparticles for fi/mri dual-modal imaging for the therapy in pancreatic cancer. Besides, Lu et al. [14] investigated some recent advancements in the hybrid cell membrane-coated NPs (HM/NPs) and their potential applications for the treatment of Cardiovascular diseases (CVDs). Then, they developed an engineered hybrid cell membrane nanosystem for treating cardiovascular diseases.

Also, high biocompatibility, high serum stability and solubility, getting away from immune system clearance (lymphocyte-macrophage), getting away from clearance of liver, lung, and kidney, ignoring drug efflux capacity, avoiding multidrug resistance, etc., are other properties of NPs in delivery of therapeutics to specific tissues and cells in the human body [14–16]. Restricted dose usage of NP-based DDSs and declining the treatment period are other advantages of this approach that have attracted the attention of researchers and clinicians [17].

Among NPs, polymeric NPs such as chitosan (CS) and polyamidoamine (PAMAM) NPs are potential materials for DDS which have been approved by the Food and Drug Administration (FDA) of the USA. CS (poly [β-(1–4)-linked-2-amino-2-deoxy-D-glucose]) NPs are bioavailable biopolymers extracted from chitin [11, 18]. Besides, the biomedical applications of CS NPs are in the field of regenerative medicine, biosensors, etc [19]. PAMAM G4 NPs are nano-size, three-dimensional, and hyper-branched chemopolymers with highly available surface amine groups [20]. The surface amino groups of CS and PAMAM NPs have led to their excellent solubility, serum, stability, and capacity to surface modification [21]. Forming polyvalent interactions with therapeutics, high drug loading capacity, controlled drug release, and enhanced permeability and retention (EPR) effect are the main aspects of these NPs [22]. Moreover, recent studies have highlighted the role of nanoprobes in improving diagnostic and therapeutic precision through simultaneous drug delivery and molecular imaging. By exploiting the enhanced permeability and retention (EPR) effect, nanoprobes can preferentially accumulate within tumor tissues, enabling targeted delivery, real-time monitoring, and controlled release of therapeutic agents. Such multifunctional platforms hold significant promise for advancing cancer theranostics and minimizing systemic side effects.On the other hand, potential therapeutics, such as sodium butyrate (Na $OOCCH_2CH_2CH_3$: NB) which is a type of bioactive drug, can use as inhibitor of cancer cells. NS can suppress the vascular endothelial growth factor (VEGF) by blocking histone deacetylases (HDACs) and VEGFR-mediated angiogenesis. This bioactive can also block the cell cycle in the G2/M phase mediating protein kinase B (Akt) and inhibiting Bcl2, IL6, and IL17 molecules which are correlated with angiogenesis, cell cycle arrest, and apoptosis Moreover, magnetic (Fe_2O_3) NPs along with therapeutics can apply for combinational therapy [23–26].

Here, it is worthwhile to mention that although Fe_2O_3 NPs have been employed in photothermal therapy (PTT) under NIR laser irradiation, their combinational impact on the suppression of cancer cells can be evaluated accompanied by NB without PTT [27]. In this paper, CS-PAMAM nanocarrier was developed for the delivery of NB and Fe_2O_3 NPs to colorectal cancer cells. After fabricating CS-PAMAM-NB-Fe_2O_3, analytical devices such as FT-IR, TGA, DLS, and TEM were employed for qualifying and quantifying DDS. Then, NB and Fe_2O_3 contents of the nanocarrier were evaluated, and NB release was

investigated in vitro. Next, cell viability assay and gene expression (qRT-PCR) technique were applied for studying the potency of fabricated DDS in suppressing the growth of SW480 cancer cells and inducing apoptosis.

Materials and methods

Materials and apparatus

CS (Mw: 50000 to 190000 Da; Viscosity: 20–300 cp.), polyamidoamine G4 (PAMAM G4) dendrimer (molecular weight: 14.215 $g.mol^{-1}$), ferrous chloride tetrahydrate ($FeCl_2{\cdot}4H_2O$), ferric chloride hexahydrate ($FeCl_3{\cdot}6H_2O$), sodium butyrate (NB), sodium tripolyphosphate (TPP), dimethyl formamide (DMF), di-methyl-sulphoxide (DMSO), N-Hydroxysuccinimide (NHS), and 1-ethyl-3-(3-dimethylaminopropyl)-carbodi-imide hydrochloride (EDC), FBS, and MTT (3-(4, 5-Dimethyl thiazol-2-yl)–2,5-diphenyl tetrazolium bromide) were purchased from Sigma Aldrich. The human SW480 colon cancer cell lines and human MSC (mesenchymal stem cell) normal cell lines were bought from the Institute of Pasteur, Iran.

Spectroscopic assessment of synthesis was implemented via Fourier Transform Infrared (FT-IR) spectrometer (Perkin-Elmer 843), NanoDrop 2000c UV–Vis spectrophotometer (Thermo Scientific), Dynamic Light Scattering (DLS) spectrophotometer (NanoBrook 90 Plus; Brookhaven, USA), and Transmission Electron Microscopy (TEM) (Philips EM 208 S; Netherlands).

Zeta potential and particle size distribution were measured using a Zetasizer Nano ZS (Malvern Instruments, UK) at 25 °C in distilled water (pH 7.4). The polydispersity index (PDI) was determined to assess particle uniformity.l.

Synthesis of carboxylated-chitosan

Carboxylated-CS (C-CS) was synthesized as the following procedure. 80 mg of CS was dissolved in 8 mL of acetic acid (1%) under stirring at 70 rpm for 10 h at room temperature. Then, NaOH (1 mM) solution prepared and dropwise to the CS-containing solution until attaining precipitation. In the next step, the precipitate was washed with deionized water three times and centrifuged at 6000 rpm followed by submerging the CS precipitate in 15 mL of isopropanol for further rinsing. Afterward, 10 mg of NaOH salt in it and the solution was stirred at 120 rpm and room temperature for 3 h. Thereafter, C-CS was prepared by dissolving 8 mg of chloroacetic acid in 4 mL isopropanol and adding it to the prepared CS solution. The mixture was stirred at 70 rpm for 10 h at dark conditions and room temperature. Eventually, the C-CS was rinsed with a 3:1 ratio of water and ethanol three times and saved at 4 °C for analytical assessments and biomedical tests.

Synthesis of PAMAM-conjugated Chitosan

In this phase, PAMAM G4 dendrimers were conjugated to C-CS by esterification reaction with NHS/EDC and formation of amid bond as the following procedure. Practically, 7 mg of PAMAM was solubilized in 8 ml of DI water. Then, 10 mL of 0.3 mM EDC and 10 mL of 0.1 mM NHS were separately prepared and combined with each other followed by adding to the prepared C-CS solution (1% acetic acid) under stirring at 80 rpm for 5 h. NHS/EDC serves as an activator of carboxylic groups in C-CS. In what follows, the prepared C-CS solution was transferred to the prepared PAMAM G4 solution drop by drop under stirring at 80 rpm at room temperature overnight. Whole reactions were carried out under a nitrogen atmosphere and light-protected conditions in this section. Ultimately, the PAMAM-CS solution was purified using a dialysis membrane in DI water (3 times) overnight to separate excessive reactants. After purification, the nanocarrier was recovered for analytical assessment and biomedical tests.

NB and Fe_2O_3 loading into PAMAM-chitosan

The NB and Fe_2O_3 were entrapped in the PAMAM-CS nanocarrier by the gelation/polyelectrolyte complexation method [28]. For this goal, firstly magnetic NPs were synthesized as the following approach. For the synthesis of magnetic NPs, Strober [29] approach was used. Briefly, 1 g ferric chloride hexahydrate and 0.5 g ferrous chloride tetrahydrate were dissolved in the mixture of 3 mL 2-propanol and 6 mL ethanol. Next, 8 mL DI and 25 mL 25% (v/v) ammonia solution were transferred to the prepared mixture of ferric chloride hexahydrate and ferrous chloride tetrahydrate under stirring at 150 rpm and a temperature of 85 °C for 5 h.

On the other hand, 5 mg of the NB was solubilized in 5 mL of DI water under 80 rpm stirring for 5 h to prepare a homogenous bioactive solution. Thereafter, the NB and Fe_2O_3-containing solutions were added to 5 mL of PAMAM-CS (3×10^{-4} M) at 37 °C under stirring at 90 rpm overnight. Then, 1 mL of TPP (1 mg/mL) was dropwise to the mixture under ultra-sonication circumstances to form globular nanocarriers. Subsequently, the NB and Fe_2O_3-entrapped nanocarrier was centrifuged at 10,000 rpm to separate unloaded bioactive. The purification was triplicated and the nanocarrier was recovered for analytical assessment and biomedical tests.

Characterization of syntheses

The characterization of synthesized nanocarriers was performed using the FT-IR, DLS, TEM, and TGA devices as the following procedures. The efficiency of synthesized samples, including CS, CS-PAMAM, CS-PAMAM-Fe_2O_3, and CS-PAMAM-Fe_2O_3-NB, was evaluated by means of FT-IR spectroscopy which implemented

applying the pellet procedure with the KBr procedure in the transmittance mode at the wavelength of 400 to 4000 cm^{-1}. The hydrodynamic diameter of specimens was measured via a DLS spectrophotometer using freshly prepared samples and after ultrasonication at 37 °C for 15 min. This test was performed at 37 °C in a quartz cuvette using nM concentrations. The TEM device was applied for determining the size and morphology of samples using a freshly prepared solution. In this technique, the CS-PAMAM-Fe_2O_3-NB sample was dispersed onto a copper grid, dried at 25 °C, and the extra liquid absorbed using filter paper followed by taking the image of the sample at 120 kV accelerating voltage. The TGA approach was conducted for investigating the thermal stability and therapeutics content of samples using 5 mg of nanocarriers and heating at a temperature range between 50 and 600 °C. This test was performed at a 10 °C/min heating rate in a pan under a constant nitrogen flow rate (40 mL/min) [30].

Drug release study

The NB release manner of the CS-PAMAM-Fe_2O_3-NB nanocarrier was scrutinized under optimal conditions in PBS as a release medium. This analysis was conducted at pH of 7.4 (serum pH) 6.0, and 5.0 (cancerous tissues pH) to evaluate the release rate of fabricated DDS. This test was done using the dialysis tube at 37 °C as the following procedure [31]. Briefly, 3 mg CS-PAMAM-Fe_2O_3-NB was solubilized in 6 mL PBS and spilled into a 12,000 Da dialysis bag (fastened with clamps at two ends). In the following, the dialysis tube was immersed in 100 mL PBS and the system located in an incubator-shaker under 120 rpm stirring and 37 °C. At pre-determined intervals of time (0.5, 1 h, 2 h, 4 h, 8 h, 16 h, 32 h, and 64 h), 10 µL of the PBS gathered and the equal values of PBS were replaced. The bioactive absorption of aliquots was quantified by Nanodrop UV–visible spectrophotometer at a wavelength of 480 nm to ascertain the release amounts.

Drug release kinetic modeling

The release kinetics of sodium butyrate from Chitosan–PAMAM nanoparticles were evaluated by fitting the in vitro release data to different mathematical models including zero-order, first-order, Higuchi, and Korsmeyer–Peppas equations. The model with the highest correlation coefficient (R^2) was considered to best describe the release mechanism.

Cell culture

The human SW480 colon cancer cell lines and human MSC (mesenchymal stem cell) normal cell lines were prepared from the Pasture Institute of Iran. These cell lines were cultured in their medium (RPMI; Gibco, UK) supplemented with 10% FBS, 2 mM glutamine, 100 µgmL^{-1} streptomycin, and 100 IU mL^{-1} penicillin and incubation at 37 °C and 5% CO_2 to grow up.

Cell viability assay

The cancer cell suppressing performance of the synthesized CS-based samples, including the CS, CS-PAMAM, CS-PAMAM-Fe_2O_3, CS-PAMAM-Fe_2O_3-NB, pure Fe_2O_3, and pure NB was investigated on SW480 cell lines after 24 h, 48 h, and 72 h of treatments with 25 nM, 50 nM, 100 nM, and 200 nM concentrations. This assessment was done by the MTT test which is based on evaluating the activity of mitochondrial dehydrogenase in treated cells. To implement this test, cancer and normal cells were spilled in wells of 96-well plates (5000 cells/100 µL per well) and incubated at 37 °C and 5% CO_2 overnight for attachment. Thereafter, various concentrations of fabricated samples were prepared in a serum-supplemented culture medium, filtered using a 0.2 mm filter, and adjusted at pH 7.4. In the following, the prepared specimens were used for the treatment of MSC and SW480 cells at 24 h, 48 h, and 72 h of post-treatment as the following procedure. After collecting the culture medium of the plates, 150 µL serial dilutions of the samples were spilled into wells, and plates were incubated for 24, 48, and 72 h. Afterward, the medium of each well was removed and 200 µL of RPMI without serum was transferred to each well at post-treatment times. Then, 0.5 mg MTT/mL prepared in PBS at pH 7.4 was added to the wells which followed by 4 h incubation. Eventually, after collecting the suspension liquid of wells, the cells were re-suspended in 200 mL of DMSO for 10 min and incubated at light-protected circumstances and the optical density (OD) of the palates was evaluated at 570 nm using an ELISA reader to measure viable cells.

Gene expression assay

The quantitative Real-Time PCR (qRT-PCR) technique was carried out to study the relative expression level of apoptotic (Caspase-9 and Bax) and anti-apoptotic (Bcl2) genes after 24 h of treatment with IC_{50} concentration of samples in SW480 cells using Q Rotor-Gene (Qiagen, Iran). Briefly, the total RNA of treated cells was extracted by mixing SW480 cells with RNX-PLUS solution. Then, 200 µL of chloroform was added to solution, and cells were centrifuged at 13,000 rpm for 5 min at 4 °C followed by collecting the supernatant and mixing the precipitate with isopropanol. Next, centrifugation was done at 13,000 rpm for 15 min at 4 °C, the supernatant removed, and the precipitate mixed with 1 mL of ethanol 75%. In what follows, cDNA was synthesized using 1000 ng of total RNA and reverse transcription. Briefly, 10 µL of Master mix real-time, 3 µL (10 ng) RNA, and 7 µL DD water spilled to microtubes to synthesize cDNA; in the wake of this process, the qRT-PCR technique done

with a 14 µL of the reaction mixture, 1 µL of cDNA, 7 µL of low rox Master mix real-time, and 0.5 µL of forward primer (Caspase-9: 5′TGGCTCCTGGTACGTTGA3′; Bax: 5′TTTCTGACGGCAACTTCAACTG3′; Bcl2: 5′TCGCCCTGTGGATGACTGA3′) and 0.5 µL of reverse primer (Caspase-9: 5′GAAACAGCATTAGCGACCCT3′; Bax: 5′TCCAATGTCCAGCCCATGA3′; Bcl2: 5′CAGAGACAGCCAGGAGAAATCA3′). The PCR temperature was optimized by qRT-PCR device: heating at 95 °C for 10 min, 45 cycles at 95 °C for 15 s, annealing at 59 °C for 25 s, and elongation at 72 °C for 30 s and consequently, relative gene expression values were normalized to glyceraldehyde-3-phosphate-dehydrogenase (GAPDH) and data was quantified as fold change relative to the control.

Statistical analysis

The experiments were repeated three times. The statistical analyses were performed using one-way ANOVA and data reported as mean ± SD. P-value ≤ 0.05 was considered significant.

Results and discussion

Characterization of nano-complex

FT-IR analysis

FT-IR analyses of fabricated samples, including CS, C-CS, PAMAM-CS, PAMAM-CS-Fe_2O_3, and PAMAM-CS-Fe_2O_3-NB, were done to confirm the synthesis quality of CS-based NP and its derivatives. Figure 1 demonstrates the results of this analysis. As can be seen, the characteristic peaks at around 3437 cm^{-1} (–NH_2 and –OH groups stretching vibration), 3337 cm^{-1} (O – H and N – H stretching vibrations), 1151 cm^{-1} (asymmetric stretching of – C–O – C– bridge), and 1034 cm^{-1} (C – N bond) were registered for pure CS [32]. Besides, signals at around 2800 cm^{-1} to 3000 cm^{-1} were assigned to CH, CH_2, and CH_3 stretching vibrations in the CS specimen while the absorption peaks at around 1639 cm^{-1} (C = O), 1388 cm^{-1} (C – N stretching), and 1068 cm^{-1} (– O stretching vibrations) were indicators of CS [33]. Regarding the C-CS sample, the characteristic peaks from 2923 cm^{-1} to 2875 cm^{-1} were associated with C-H stretching vibrations in C-CS while a signal at around 1708 cm^{-1} was recorded due to the presence of the carboxyl group in C-CS [34]. For the PAMAM-CS sample, the peaks of PAMAM G4 were revealed at around 1046 cm^{-1} to 1112 cm^{-1} and 1214 cm^{-1} which were detected owing to the C–C bending and C–O stretching vibration, respectively [35]. Also, the absorption peaks achieved at around 1577 cm^{-1}, 1422 cm^{-1}, and 1320 cm^{-1} were indicators of N–H bending of N substituted amide whereas signals at around 3300 cm^{-1} and 3100 cm^{-1} were responsible for N–H stretch of amines and anti-symmetric N–H stretch of substituted primary amine, respectively [36]. Regarding the PAMAM-CS-Fe_2O_3 sample, the peaks at around 560 cm^{-1} to 590 cm^{-1} were attributed to Fe – O groups in Fe_2O_3 NPs [37]. Additionally, there were some shifts in the locations of other peaks which are indicators of magnetic NPs in the body of CS-PAMAM. About the PAMAM-CS-Fe_2O_3-NB nanocarrier, the absorption peaks at around 1728 cm^{-1} and from 2871 cm^{-1} to 2957 cm^{-1} corresponded for C = O stretching and the C–H stretching of NB bioactive which verifies the presence of NB.

DLS and TEM analyses

The DLS and TEM analyses were used for determining the hydrodynamic size, (PDI), and morphology of fabricated nanocarriers. For DLS analysis, the hydrodynamic diameter and polydispersity index (PDI) of PAMAM-CS, PAMAM-CS-Fe_2O_3, and PAMAM-CS-Fe_2O_3-NB samples was ascertained using DLS (Fig. 2). According to the outputs, the hydrodynamic diameter of the PAMAM-CS sample was measured at about 210 nm while it determined at around 234 nm after magnetic NPs entrapment which shows an increase of 24 nm in diameter. Besides, after the entrapment of NB, the hydrodynamic diameter enhanced by 4 nm and reached 238 nm. Intermolecular interactions between the surface functional groups of PAMAM-CS and bioactive (Fe_2O_3 and NB) could be the main reason for the size increase after entrapment. These Intermolecular interactions are including the formation of π-π interaction and electrostatic and hydrogen bonds which can play a prominent role in therapeutics release [38]. The PDI of all specimens was measured at about less than 0.2, which demonstrates the monodispersity of nanocarriers. Regarding the TEM analysis, the image of the PAMAM-CS-Fe_2O_3-NB sample exhibited a diameter between 40 nm and 65 nm and a semi-globular shape which verifies the nano-meter size of DDS. The vasculature size of cancer tissues is from 200 nm to 700 nm and a diameter less than 200 nm is appropriate for efficient drug delivery [39].

The physicochemical properties of the synthesized Chitosan–PAMAM nanoparticles were further characterized by dynamic light scattering (DLS) and zeta potential analysis. The average hydrodynamic diameter was found to be 142.6 ± 5.3 nm with a polydispersity index (PDI) of 0.186, confirming a monodisperse population suitable for biological applications. The surface charge of the nanoparticles was + 27.4 ± 2.1 mV, indicating strong electrostatic stability and effective surface functionalization by the chitosan component. No visible aggregation or significant shift in particle size was observed after 7 days of storage in phosphate-buffered saline (pH 7.4), suggesting good colloidal stability. These physicochemical characteristics are crucial for predicting the in vivo

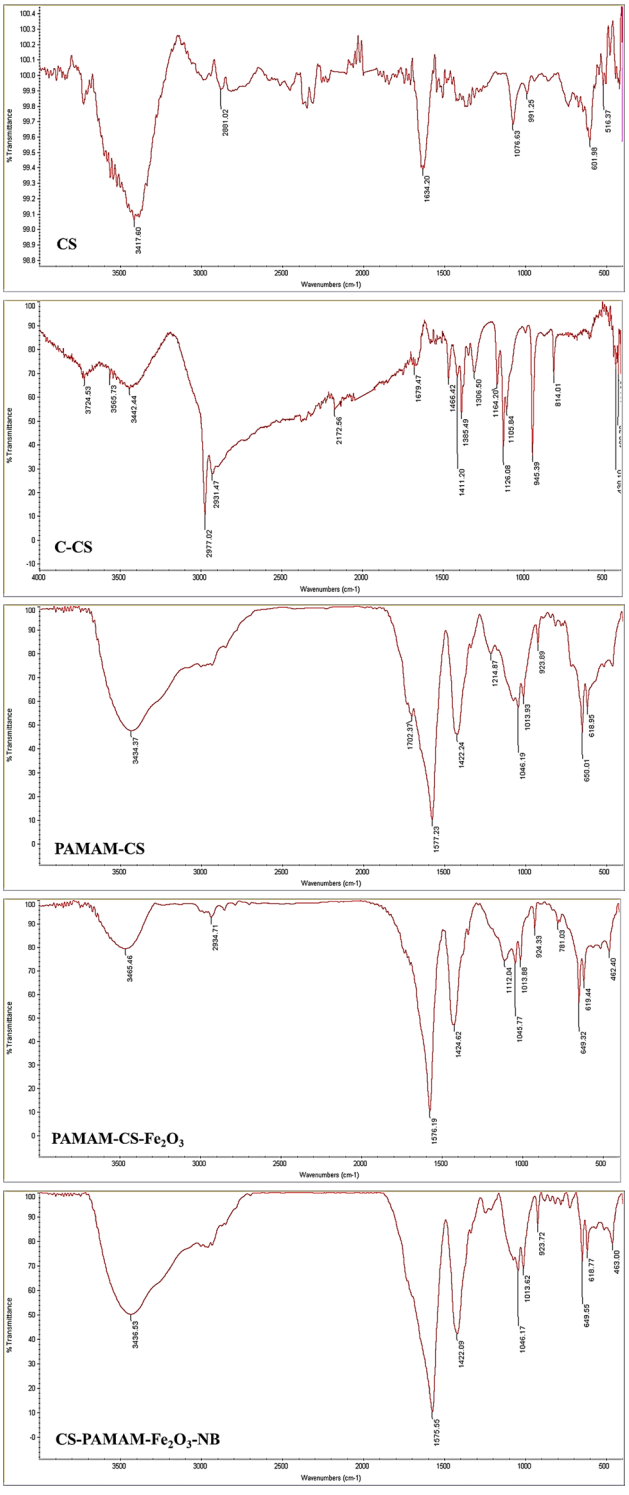

Fig. 1 The FT-IR spectra of CS, C-CS, PAMAM-CS, PAMAM-CS-Fe_2O_3, and PAMAM-CS-Fe_2O_3-NB samples. The peaks at around 3437 cm^{-1} (–NH_2 and –OH groups stretching vibration), 3337 cm^{-1} (O–H and N–H stretching vibrations), 1151 cm^{-1} (asymmetric stretching of –C–O–C– bridge), and 1034 cm^{-1} (C–N bond) were indicators of CS in pure CS graph. The peaks of PAMAM G4 were recorded at 1046 cm^{-1} to 1112 cm^{-1} and 1214 cm^{-1} owing to the C–C bending and C–O stretching vibration, respectively. For the PAMAM-CS-Fe_2O_3nanocarrier, the peaks at around 560 cm^{-1} to 590 cm^{-1} were assigned to Fe–O groups in Fe_2O_3 NPs

performance and interaction of nanoparticles with biological membranes.

TG analysis

TG analysis was performed for surveying the thermal stability, physical status, and drug content of synt5ehsized samples (PAMAM-CS, PAMAM-CS-Fe_2O_3, and PAMAM-CS-Fe_2O_3-NB) [30]. Figure 3 indicates the results of this test. As can be seen, there were two weight-loss stages for the samples. The first weight loss of the samples (3% to 15%) was registered at around 80 °C to 100 °C which was due to the water evaporation of samples. The second one was started at around 130 °C (PAMAM-CS) and 150 °C (for PAMAM-CS-Fe_2O_3 and PAMAM-CS-Fe_2O_3-NB) at which 63%, 76%, and 84% weight losses occurred for PAMAM-CS, PAMAM-CS-Fe_2O_3, and PAMAM-CS-Fe_2O_3-NB samples, respectively. These considerable weight losses were due to the burning of material in the compartment of specimens. On the other hand, the difference in total weight losses of specimens can consider as bioactive content; as the Fe_2O_3 content of PAMAM-CS-Fe_2O_3 was measured at about 23% and the difference in weight loss values of PAMAM-CS-Fe_2O_3 and PAMAM-CS-Fe_2O_3-NB samples was contemplated as NB content PAMAM-CS-Fe_2O_3-NB which was about 3%. Bioactive drug content is a vital issue correlated with novel DDSs and high values of therapeutics in the body of DSSs play a major role in transporting high values of bioactive to cancer tissues and cells [40].

Drug release profile

The in vitro drug release profile of the PAMAM-CS-Fe_2O_3-NB nanocarrier was investigated in PBS solution. In this assessment, the release of NB was studied at various pHs 7.4 (as physiologic pH) 6.0, and 5.0 (as the simulation of pH in cancerous tissues and cells) and different times (0.5 h to 64 h). Figure 4 indicates the release data of NB. Based on the results, the release manner of NB from PAMAM-CS-Fe_2O_3-NB was slowed which confirms the effect of fabricated nanocarrier on controlled and constant release of NB over the determined period of time. For example, 4% of NB release was observed within the first 2 h while it was 43% for pure NB which shows more than 10 folds slower NB release from PAMAM-CS-Fe_2O_3-NB. Also, about 12% and 69% of drug releases were measured for PAMAM-CS-Fe_2O_3-NB and pure NB, respectively. On the other hand, NB release from nanocarrier was faster in both acidic pHs than normal pH which approves the impact of acidic pH in increasing the release rate of the drug from nanocarrier. For instance, the NB release was 29% and 35% within 2 h of incubation at pH 6.0 and 5.0, respectively whereas it was only about 12% at neutral pH. Protonation of amine groups of PAMAM and CS at acidic pHs is the main reason for

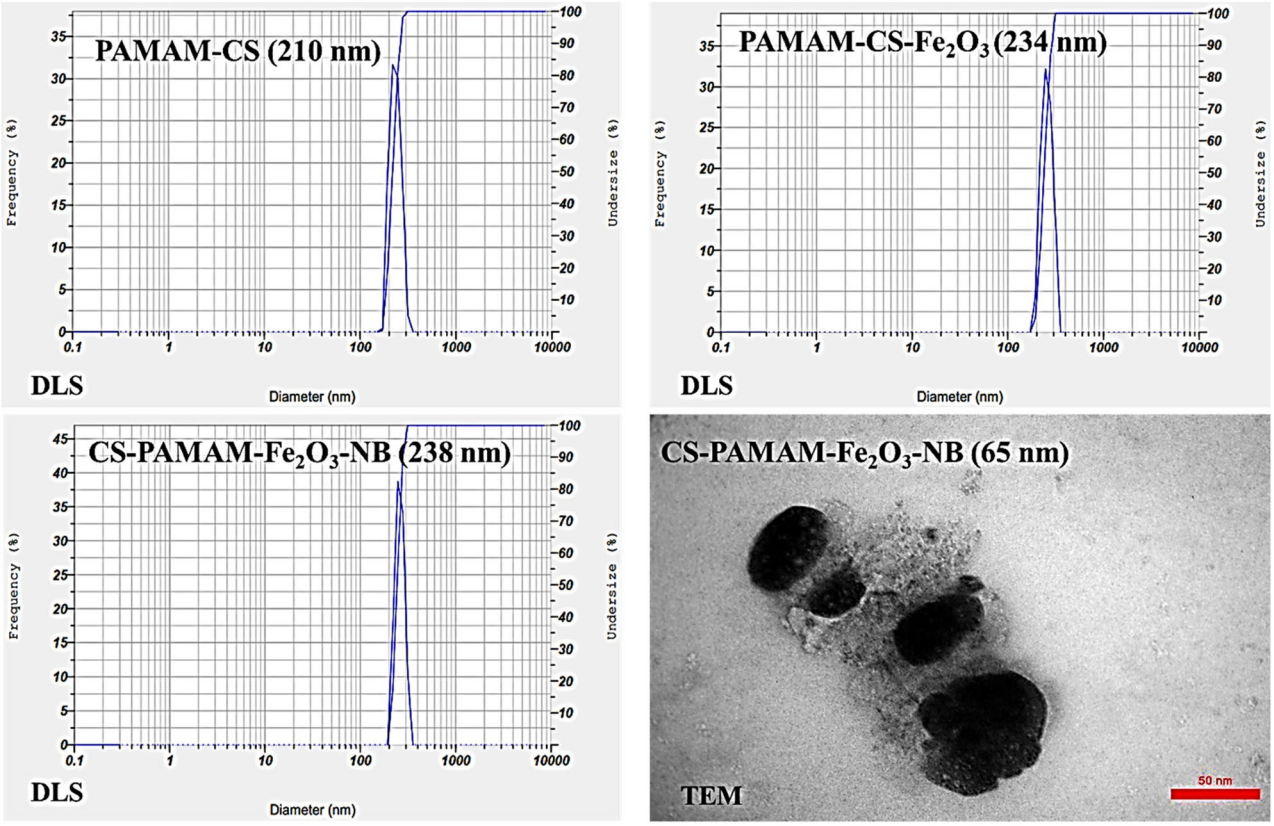

Fig. 2 The DLS and TEM analyses of fabricated nano-carriers, including PAMAM-CS, PAMAM-CS-Fe_2O_3, and PAMAM-CS-Fe_2O_3-NB. As indicated, the hydrodynamic diameter of PAMAM-CS, PAMAM-CS-Fe_2O_3, and PAMAM-CS-Fe_2O_3-NB samples was ascertained at around 210 nm, 234 nm, and 238 nm. TEM image show a size range of 40 nm to 65 nm in diameter

the fast drug release [41]. Besides, the fast drug release at acidic pHs is important since the early and late endosomes have acidic environments. Also, the cancer tissues due to the high rate of metabolism have acidic pHs [42].

The cumulative release profiles of sodium butyrate from Chitosan–PAMAM nanoparticles were fitted to common kinetic models to elucidate the release mechanism. The release behavior followed the Higuchi model (R^2 = 0.987), indicating that diffusion was the predominant mechanism governing drug release. Further analysis using the Korsmeyer–Peppas equation yielded an exponent value ($n = 0.46$), suggesting Fickian diffusion as the controlling process. This result is consistent with the porous and hydrophilic nature of the chitosan-based matrix, which facilitates the gradual diffusion of the entrapped drug molecules.

MTT analysis

The MTT assay was employed for scrutinizing the toxic impact of CS-based DDSs, including CS, CS-PAMAM, CS-PAMAM-Fe_2O_3, CS-PAMAM-Fe_2O_3-NB, pure Fe_2O_3, and pure NB, on SW480 cell lines after 24 h, 48 h, and 72 h of treatments with 25 nM, 50 nM, 100 nM, and 200 nM concentrations. MSC normal cell lines used as a control. Figure 5 exhibits the cell viability values. As can be seen, it revealed that the CS specimen had higher biocompatibility and biodegradability compared with other samples in both cell lines; as by increasing the concentration of this sample, the cell viability values were enhanced at three times [19, 22]. The cell viability values for pure CS were determined between 82% and 95% for 25 nM and 200 nM concentrations in both cell lines, respectively. Regarding the rest of the samples, the cell viability values had a reverse correlation with concentrations. As by raising the concentration of samples, the cell viability values decreased. For instance, the CS-PAMAM sample led to cell viability values from 82% (25 nM) to 77% (200 nM) after 24 h treatment in SW480 cells. Regarding the CS-PAMAM-Fe_2O_3 sample, higher cytotoxicity was observed at higher concentrations, with 75% (24 h), 74% (48 h), and 71% (72 h) in SW480 cells.

Totally, the cytotoxicity of the CS-PAMAM-Fe_2O_3 sample was higher than that of the CS-PAMAM sample which indicates the impact of iron oxide in the suppression of SW480 cells. For the CS-PAMAM-Fe_2O_3-NB nanocarrier, the cell viability value was quantified at around 10% while it was 43% for pure NB at 24 of post-treatment time in SW480 cells which verifies the

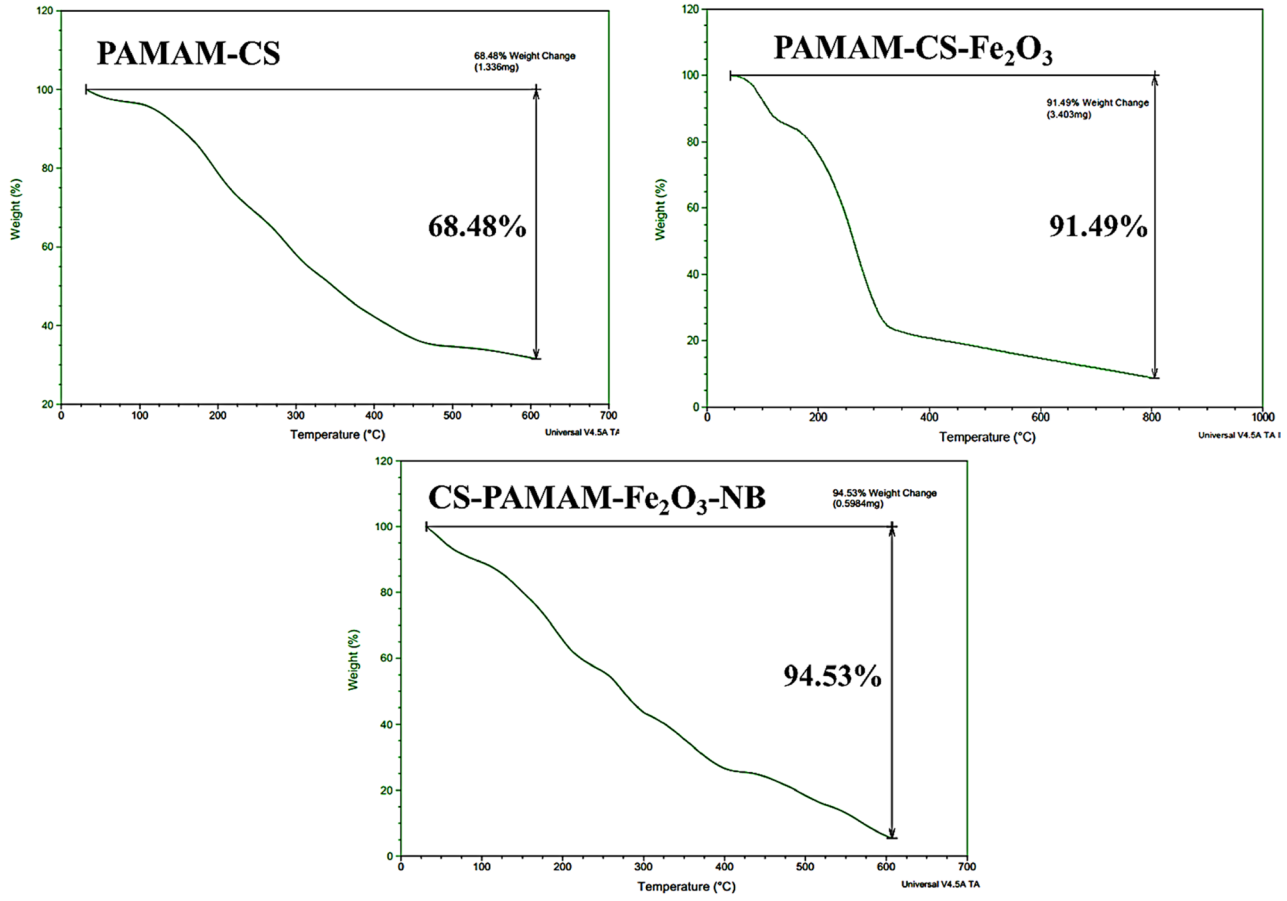

Fig. 3 The TG analysis of PAMAM-CS, PAMAM-CS-Fe_2O_3, and PAMAM-CS-Fe_2O_3-NB samples. High thermal stability was detected for samples. The Fe_2O_3 and NB contents of samples were measured at about 23% and 3%, respectively

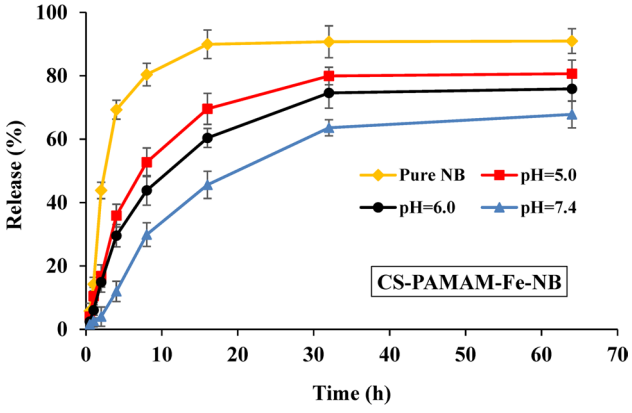

Fig. 4 The drug release manner of PAMAM-CS-Fe_2O_3-NB nanocarrier and pure NB at various pHs (7.4, 6.0, and 5.0). controlled release was measured for PAMAM-CS-Fe_2O_3-NB at pH 7.4 while it was very fast for pure NB. The acidic environment resulted in the protonation of PAMAM-CS-Fe_2O_3-NB and the fast rate of NB release profile

effect of nanoparticle-based DDS in efficient suppression of cancer cells compared with NB [2, 34]. About 8% and 7% cell viabilities were also detected in cancer cells after 48 h and 72 h of treatments with 200 nM of CS-PAMAM-Fe_2O_3-NB, respectively. Generally, the CS-PAMAM-Fe_2O_3-NB nanocarrier had about 4 folds to 6 folds better toxic performance on SW480 cells than pure NB at all treatment times. On the other side, CS-PAMAM-Fe_2O_3-NB did not have higher cytotoxicity on normal cells compared with pure NB. For instance, 76% and 44% cell viabilities were attained after 24 h treatment with 200 nM of CS-PAMAM-Fe_2O_3-NB and pure NB on MSC normal cells, respectively which depicts the positive impact of biocompatible nanocarrier on normal cells [22]. The IC_{50} values were determined for 25 nM of CS-PAMAM-Fe_2O_3-NB at all treatment times. The results of our work were in accordance with the findings of research by Song et al., in which they developed the iron oxide-polypyrrole-polyethylene glycol polymeric nanocarrier for the inhibition of cancer cells [43]. They demonstrated that Fe_2O_3-loaded DDS could effectively decline the growth of breast cancer cells to less than 20% under laser irradiation while pure Fe_2O_3 did not have higher toxicity on cancer cells. Our results indicated that fabricated nanocarrier can potentially suppress the growth of colon cancer cells. NB was the major agent in inducing toxicity

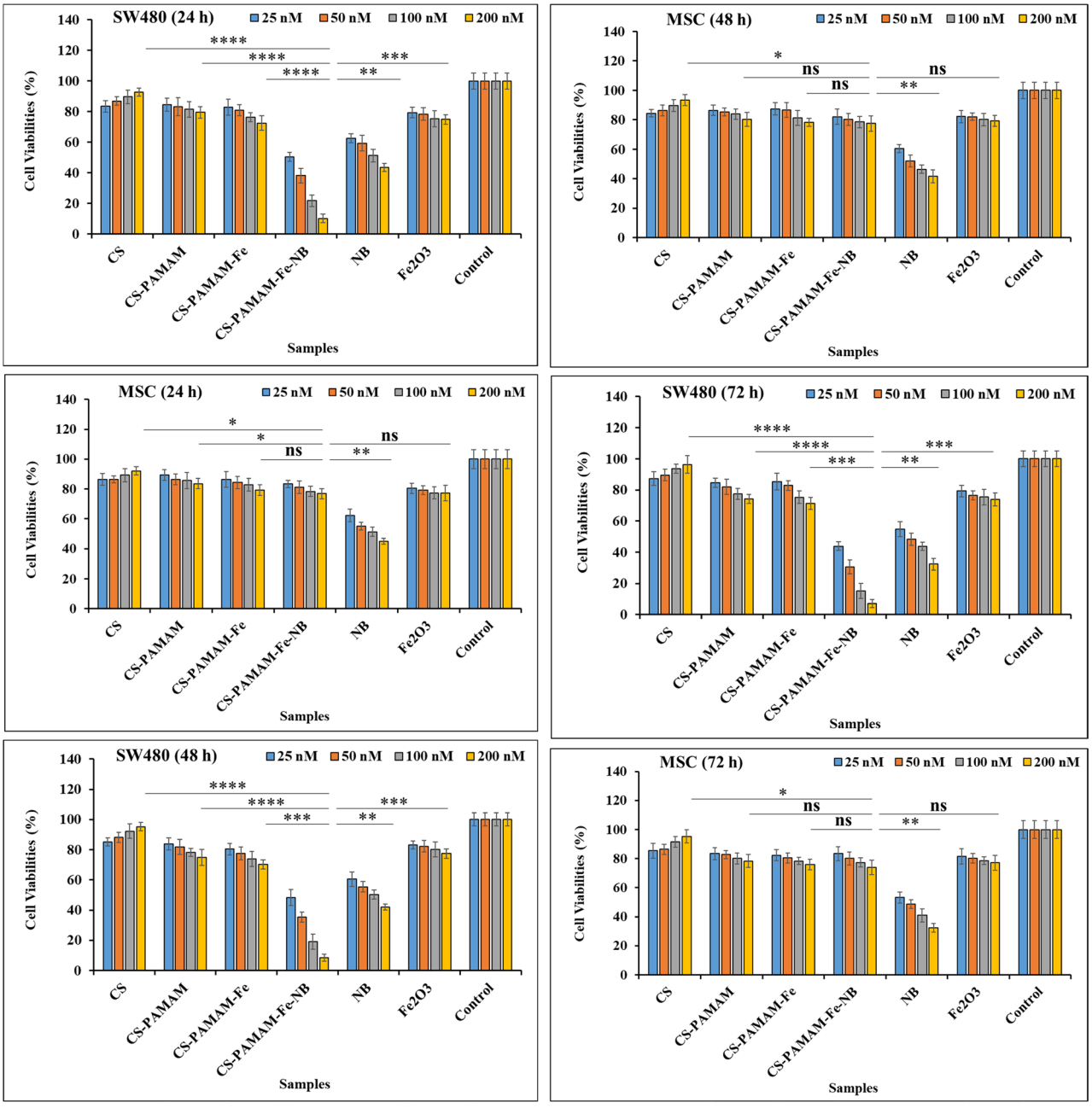

Fig. 5 Cell viability of SW480 colon cancer cells and MSC normal cells after 24 h, 48 h, and 72 h of treatment with CS, CS-PAMAM, CS-PAMAM-Fe_2O_3, CS-PAMAM-Fe_2O_3-NB, pure Fe_2O_3, and pure NB. Higher cytotoxicity was observed for the CS-PAMAM-Fe_2O_3-NB sample on SW480 cells which was less than 10% at three treatment times. The cytotoxicity of pure NB was considerably lower than that of the CS-PAMAM-Fe_2O_3-NB sample

and cell death on SW480 cells and Fe_2O_3 had only a low toxic effect on the growth of cancer cells.

Gene expression analysis

The expression values of apoptotic and anti-apoptotic genes were investigated after 24 h treatment with CS-PAMAM-Fe_2O_3, CS-PAMAM-Fe_2O_3-NB, and pure NB samples on SW480 cells using the qRT-PCR technique. The IC_{50} values were applied for this test. In this assay, the relative expression values of apoptotic (Caspase9 and Bax) and anti-apoptotic (Bcl2) genes evaluated. Figure 6 shows the data after treatment with 25 nM concentrations of CS-PAMAM-Fe_2O_3, CS-PAMAM-Fe_2O_3-NB, and pure NB formulations. While the Bax gene expression mediates apoptosis by affecting the mitochondrial outer membrane, the Caspase9 gene induces apoptosis via the mitochondria-dependent cytochrome c release pathway [44–47]. From Fig. 6, it is crystal clear that the CS-PAMAM-Fe_2O_3-NB sample had higher effect on inducing apoptosis genes expression, with about 10.5

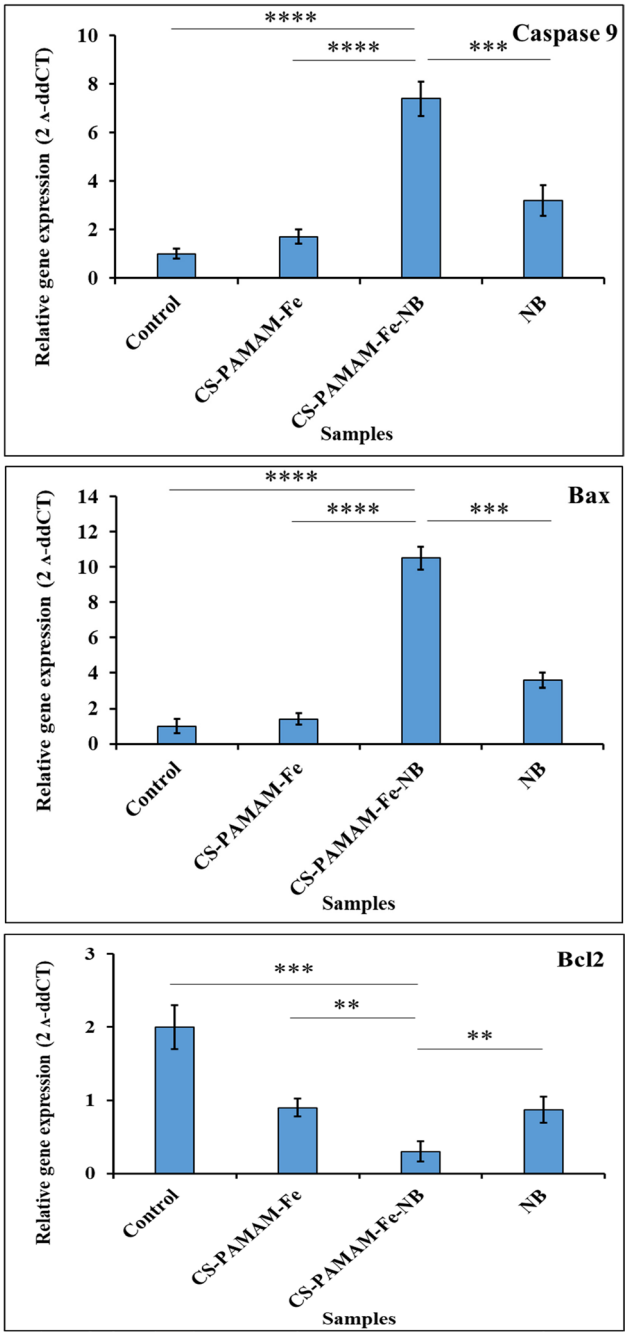

Fig. 6 The relative gene expression levels of apoptotic (Caspase9 and Bax) and anti-apoptotic (Bcl2) genes after 24 h treatment with 25 nM concentrations of CS-PAMAM-Fe_2O_3, CS-PAMAM-Fe_2O_3-NB, and pure NB samples on SW480 cells. As indicated, the CS-PAMAM-Fe_2O_3-NB sample had a higher impact on inducing the expression of apoptotic genes and inhibition of anti-apoptotic gene

folds and 7.4 folds enhancement in the expression values of Bax and Caspase9 genes compared with control, respectively. Pure NB exhibited a lower (with about two to three folds) impact on the expression levels of Bax and Caspase9 than the CS-PAMAM-Fe_2O_3-NB sample which demonstrates the high potency of nanocarrier in inducing apoptosis in SW480 cells. On the other hand, CS-PAMAM-Fe_2O_3-NB led to suppression of the expression of the Bcl2 gene by about 6.5 folds and 2.5 folds compared with control and pure NB, respectively. The results of this test were in line with MTT assay outputs.

Although the present work demonstrates the promising potential of sodium butyrate-loaded Chitosan–PAMAM nanoparticles in suppressing colorectal cancer cell proliferation in vitro, it is important to note that no in vivo or pharmacokinetic validation was performed in this study. Therefore, the translational relevance of the findings remains limited. Future investigations will include in vivo biodistribution, pharmacokinetic profiling, and therapeutic efficacy assessments in suitable animal models to confirm tumor-specific accumulation, systemic safety, and the long-term biocompatibility of the proposed nanocarrier system.

In addition to the need for in vivo validation, several practical challenges must be considered before clinical translation of Chitosan–PAMAM-based nanocarriers. Nanoparticle aggregation in physiological ionic conditions may reduce their stability and alter biodistribution, potentially leading to rapid clearance or unexpected accumulation. While both chitosan and PAMAM are known for their biodegradability and biocompatibility, controlling the degradation rate is crucial to maintain sustained release while avoiding premature breakdown. Moreover, systemic clearance through the reticuloendothelial system (RES) may limit the circulation time of the nanoparticles. Future formulations could incorporate surface PEGylation or targeted ligand modification to improve colloidal stability, prolong systemic circulation, and enhance tumor-specific accumulation.

Conclusion

In this work, we developed CS-based DDSs against colorectal cancer. As CS-PAMAM G4 nanocarriers were synthesized for efficient delivery of NB and Fe_2O_3 NPs. Afterward, a sort of analytical device, including FT-IR, DLS, TEM, and TGA, was applied for the characterization of the fabricated DDS. The nanometric size, high therapeutics content, controlled and pH-sensitive NB release were measured for the CS-PAMAM-Fe_2O_3-NB nanocarrier. In what follows, MTT assay and qRT-PCR technique were applied for determining cancer cell suppression and apoptosis-inducing capability of CS-PAMAM-Fe_2O_3-NB. The results of these biomedical tests have approved potential the ability of the synthesized DDS in the inhibition of colorectal cancer cells. High biocompatibility was shown in MSC normal cells which further verified the efficiency of CS-PAMAM-Fe_2O_3-NB. These data have confirmed that the fabricated nanocarrier is a promising DDS for the suppression of cancer cells.

Abbreviations

NPs	Nanoparticles
CS	Chitosan
PAMAM	Polyamidoamine
NB	Sodium butyrate
FT-IR	Fourier transform infrared
TGA	Thermogravimetric analysis
DLS	Dynamic light scattering
TEM	Transmission electron microscopy
DDS	Drug delivery system

Acknowledgements
Not applicable.

Authors' contributions
Ruaa Mahdi Mayih Al-Zihaymee: wrote the main manuscriptJavad Mohammadnejad: Formal analysisAsghar Narmani: SoftwareHanieh Jafari : MethodologyGülüzar Özbolat: edited the final draftAmin Daemi: supervisorYusuf Döğüş: edited the final draftSeyyedeh Touran Hosseini: edited the finalAll authors reviewed the manuscript."

Funding
This research received no external funding.

Data availability
The required data are available from the corresponding author upon the reasonable request.

Declarations

Competing interests
The authors declare no competing interests.

Received: 13 September 2025 / Accepted: 10 November 2025
Published online: 29 December 2025

References

1. Morgan E, et al. Global burden of colorectal cancer in 2020 and 2040: incidence and mortality estimates from GLOBOCAN. Gut. 2023;72(2):338–44.
2. Yousefi M, Narmani A, Jafari SM. Dendrimers as efficient nanocarriers for the protection and delivery of bioactive phytochemicals. Adv Colloid Interface Sci. 2020;278:102125.
3. Wong MC, et al. Differences in incidence and mortality trends of colorectal cancer worldwide based on sex, age, and anatomic location. Clin Gastroenterol Hepatol. 2021;19(5):955-966. e61.
4. Xi Y, Xu P. Global colorectal cancer burden in 2020 and projections to 2040. Transl Oncol. 2021;14(10):101174.
5. Naderlou E, et al. Enhanced sensitivity and efficiency of detection of *Staphylococcus aureus* based on modified magnetic nanoparticles by photometric systems. Artif Cells Nanomed Biotechnol. 2020;48(1):810–7.
6. Yin T, et al. Engineering bacteria and bionic bacterial derivatives with nanoparticles for cancer therapy. Small. 2022;18(12):2104643.
7. Amini A, et al. Bio-barcode technology for detection of *Staphylococcus aureus* protein A based on gold and iron nanoparticles. Int J Biol Macromol. 2019;124:1256–63.
8. Wang S, et al. Nanoparticle-based medicines in clinical cancer therapy. Nano Today. 2022;45:101512.
9. Narmani A, et al. Gadolinium nanoparticles as diagnostic and therapeutic agents: their delivery systems in magnetic resonance imaging and neutron capture therapy. J Drug Deliv Sci Technol. 2018;44:457–66.
10. Tu L, et al. miRNA-218-loaded carboxymethyl chitosan-Tocopherol nanoparticle to suppress the proliferation of Gastrointestinal stromal tumor growth. Mater Sci Engineering: C. 2017;72:177–84.
11. Alnasraui AH, Joe IH, Al-Musawi S. Investigation of dextran-coated magnetic nanoparticles encapsulated by medication and modified with folate for targeted drug delivery: invitro and Docking studies. Mater Chem Phys. 2024;321:129446.
12. Alnasraui AH, Joe IH, Al-Musawi S. Investigation of Folate-Functionalized Magnetic-Gold nanoparticles based targeted drug delivery for liver: in Vitro, in vivo and Docking studies. ACS Biomaterials Sci Eng. 2024;10(10):6299–313.
13. Ren S, Song L, Tian Y, Zhu L, Guo K, Zhang H, Wang Z. Emodin-Conjugated pegylation of Fe3O4 nanoparticles for FI/MRI Dual-Modal imaging and therapy in pancreatic cancer. Int J Nanomed. 2021;16:7463–78. PMID: 34785894; PMCID: PMC8579871.
14. Lu H, Jiang Y, Luo R, Zhou D, Zheng F, Shi L, Zhang H, Wang Y, Xu X, Zou R, Zhou Y, Ren S, Wang X, Sang H. Engineered hybrid cell membrane nanosystems for treating cardiovascular diseases. Mater Today Bio. 2025;33:101992. PMID: 40673130; PMCID: PMC12264635.
15. Wu D, et al. Chitosan-based colloidal polyelectrolyte complexes for drug delivery: a review. Carbohydr Polym. 2020;238:116126.
16. Narmani A, Yavari K, Mohammadnejad J. Imaging, biodistribution and in vitro study of smart ^{99m}Tc-PAMAM G4 dendrimer as novel nano-complex. Colloids Surf B. 2017;159:232–40.
17. Lee SH, et al. Strategic approaches for colon targeted drug delivery: an overview of recent advancements. Pharmaceutics. 2020;12(1):68.
18. Mohammed MA, et al. An overview of chitosan nanoparticles and its application in non-parenteral drug delivery. Pharmaceutics. 2017;9(4):53.
19. Khalaf EM et al. Recent progressions in biomedical and pharmaceutical applications of Chitosan nanoparticles: A comprehensive review. Int J Biol Macromol. 2023;231:123354.
20. Khakinahad Y, et al. Margetuximab conjugated-PEG-PAMAM G4 nano-complex: a smart nano-device for suppression of breast cancer. Biomed Eng Lett. 2022;12(3):317–29.
21. Narmani A, et al. Targeting delivery of oxaliplatin with smart PEG-modified PAMAM G4 to colorectal cell line: in vitro studies. Process Biochem. 2018;69:178–87.
22. Narmani A, Jafari SM. Chitosan-based nanodelivery systems for cancer therapy: recent advances. Carbohydr Polym. 2021;272:118464.
23. Ren S, Song L, Tian Y, Zhu L, Guo K, Zhang H, et al. Emodin-conjugated PEGylated Fe_3O_4 nanoparticles for FI/MRI dual-modal imaging and therapy in pancreatic cancer. Int J Nanomedicine. 2021;16:7463–78.
24. Vagena I-A, Malapani C, Gatou M-A, Lagopati N, Pavlatou EA. Enhancement of EPR effect for passive tumor targeting: current status and future perspectives. Appl Sci. 2025;15(6):3189.
25. Luo S, et al. Sodium butyrate induces autophagy in colorectal cancer cells through LKB1/AMPK signaling. J Physiol Biochem. 2019;75:53–63.
26. Wang S, et al. Plasmonic copper sulfide nanocrystals exhibiting near-infrared photothermal and photodynamic therapeutic effects. ACS Nano. 2015;9(2):1788–800.
27. Liu B, et al. Magnetically targeted delivery of DOX loaded Cu 9 S 5@ mSiO 2@ Fe 3 O 4-PEG nanocomposites for combined MR imaging and chemo/photothermal synergistic therapy. Nanoscale. 2016;8(25):12560–9.
28. Yılmaz H. A pH-Sensitive Chitosan/Oxidized-Kappa-Carrageenan based Nano-Antibiotic for sustained and controlled release of amoxicillin. J Macromolecular Sci Part B. 2022;61(7–8):926–41.
29. Narmani A, et al. Highly sensitive and accurate detection of vibrio cholera O1 OmpW gene by fluorescence DNA biosensor based on gold and magnetic nanoparticles. Process Biochem. 2018;65:46–54.
30. Narmani A, Mohammadnejad J, Yavari K. Synthesis and evaluation of polyethylene glycol-and folic acid-conjugated polyamidoamine G4 dendrimer as nanocarrier. J Drug Deliv Sci Technol. 2019;50:278–86.
31. Faramarzi N, et al. Synthesis and in vitro evaluation of tamoxifen-loaded gelatin as effective nanocomplex in drug delivery systems. Int J Nanosc. 2020;19(05):2050002.
32. Bandara S, et al. Synthesis and characterization of Zinc/Chitosan-Folic acid complex. Heliyon. 2018;4(8):e00737.
33. Rezvani M, et al. Synthesis and in vitro study of modified chitosan-polycaprolactam nanocomplex as delivery system. Int J Biol Macromol. 2018;113:1287–93.
34. Parveen S, Sahoo SK. Long Circulating chitosan/PEG blended PLGA nanoparticle for tumor drug delivery. Eur J Pharmacol. 2011;670(2–3):372–83.
35. Narmani A, et al. Breast tumor targeting with PAMAM-PEG-5FU-99m Tc as a new therapeutic nanocomplex: in In-vitro and In-vivo studies. Biomed Microdevices. 2020;22:1–13.
36. Fotouhi P, et al. Surface modified and rituximab functionalized PAMAM G4 nanoparticle for targeted Imatinib delivery to leukemia cells: in vitro studies. Process Biochem. 2021;111:221–9.

37. Wang S, et al. Aptamer-functionalized Chitosan magnetic nanoparticles as a novel adsorbent for selective extraction of Ochratoxin A. Int J Biol Macromol. 2020;153:583–90.
38. Moutabian H, et al. The cardioprotective effects of nano-curcumin against doxorubicin-induced cardiotoxicity: A systematic review. BioFactors. 2022;48(3):597–610.
39. Mortezaee K, et al. Synergic effects of nanoparticles-mediated hyperthermia in radiotherapy/chemotherapy of cancer. Life Sci. 2021;269:119020.
40. Huang S-J, et al. Hybrid pegylated chitosan/PLGA nanoparticles designed as pH-responsive vehicles to promote intracellular drug delivery and cancer chemotherapy. Int J Biol Macromol. 2022;210:565–78.
41. Amirishoar M, et al. Design and fabrication of folic acid-conjugated and gold-loaded Poly (lactic-co-glycolic acid) biopolymers for suppression of breast cancer cell survival combining photothermal and photodynamic therapy. J Drug Deliv Sci Technol. 2023;83:104266.
42. Ghaemi B, Javad M, Hajipour. Tumor acidic environment directs nanoparticle impacts on cancer cells. J Colloid Interface Sci. 2023;634:684–92.
43. Song X, et al. Ultra-Small iron oxide doped polypyrrole nanoparticles for in vivo multimodal imaging guided photothermal therapy. Adv Funct Mater. 2014;24(9):1194–201.
44. Westphal D, et al. Molecular biology of Bax and bak activation and action. Biochimica et biophysica acta (BBA). - Mol Cell Res. 2011;1813(4):521–31.
45. Sharifi S, et al. Doxorubicin changes Bax /Bcl-xL Ratio, Caspase-8 and 9 in breast cancer cells. Adv Pharm Bull. 2015;5(3):351–9.
46. Kamali M, Jafari H, Taati F, Mohammadnejad J, Daemi A. Synthesis of Chitosan polyethylene glycol antibody complex for delivery of Imatinib in lung cancer cell lines. J Biochem Mol Toxicol. 2024;38(8):e23787. https://doi.org/10.1002/jbt.23787.
47. Sun X, Zhai H, Chen X, Kong R, Zhang X. MicroRNA-1271 suppresses the proliferation and invasion of colorectal cancer cells by regulating metadherin/Wnt signaling. J Biochem Mol Toxicol. 2018;32(2):e22028. https://doi.org/10.1002/jbt.22028.

Publisher's Note